

UNIVERSIDADE ESTADUAL DE CAMPINAS  
SISTEMA DE BIBLIOTECAS DA UNICAMP  
REPOSITÓRIO DA PRODUÇÃO CIENTÍFICA E INTELECTUAL DA UNICAMP

**Versão do arquivo anexado / Version of attached file:**

Versão do Editor / Published Version

**Mais informações no site da editora / Further information on publisher's website:**

<https://opg.optica.org/ol/abstract.cfm?uri=ol-40-14-3332>

**DOI: 10.1364/OL.40.003332**

**Direitos autorais / Publisher's copyright statement:**

©2015 by Optical Society of America. All rights reserved.

DIRETORIA DE TRATAMENTO DA INFORMAÇÃO

Cidade Universitária Zeferino Vaz Barão Geraldo

CEP 13083-970 – Campinas SP

Fone: (19) 3521-6493

<http://www.repositorio.unicamp.br>

# Optics Letters

## Spectral engineering with coupled microcavities: active control of resonant mode-splitting

MARIO C. M. M. SOUZA,<sup>1</sup> GUILHERME F. M. REZENDE,<sup>1</sup> LUIS A. M. BAREA,<sup>1,2</sup> ANTONIO A. G. VON ZUBEN,<sup>1</sup> GUSTAVO S. WIEDERHECKER,<sup>1</sup> AND NEWTON C. FRATESCHI<sup>1,\*</sup>

<sup>1</sup>Instituto de Física Gleb Wataghin, Universidade Estadual de Campinas, 13083-970 Campinas, São Paulo, Brazil

<sup>2</sup>Departamento de Engenharia Elétrica, Universidade Federal de São Carlos, 13565-905 São Carlos, São Paulo, Brazil

\*Corresponding author: fratesch@ifi.unicamp.br

Received 28 May 2015; accepted 13 June 2015; posted 26 June 2015 (Doc. ID 240422); published 9 July 2015

**Optical mode-splitting is an efficient tool to shape and fine-tune the spectral response of resonant nanophotonic devices. The active control of mode-splitting, however, is either small or accompanied by undesired resonance-shifts, often much larger than the resonance splitting. We report a control mechanism that enables reconfigurable and widely tunable mode splitting while efficiently mitigating undesired resonance shifts. This is achieved by actively controlling the excitation of counter-traveling modes in coupled resonators. The transition from a large splitting (80 GHz) to a single-notch resonance is demonstrated using low-power microheaters (35 mW). We show that the spurious resonance shift in our device is only limited by thermal crosstalk, and resonance-shift-free splitting control may be achieved.** © 2015 Optical Society of America

**OCIS codes:** (230.4555) Coupled resonators; (130.3120) Integrated optics devices.

<http://dx.doi.org/10.1364/OL.40.003332>

The ability to tailor the spectral features of compact photonic devices is essential to address the need for complex optical responses in a wide range of applications, including optical signal processing, sensing, and nonlinear optics [1–3]. Microcavity resonant mode-splitting has been explored in these applications as a powerful tool to enable spectral engineering with low power consumption and small footprint. For example, selective mode-splitting has recently enabled four-wave mixing through dispersion compensation [4,5], carrier recycling [6], compact phase-shifters for microwave photonics [7], and the use of multiple-split resonances to overcome the trade-off between the cavity free-spectral range (FSR) and optical field enhancement [8]. The engineering of the optical phase delay through resonant mode-splitting has also been explored to demonstrate pulse delay/advancement [9].

A major limitation of spectral engineering through mode-splitting in integrated devices is its challenging control. In order

to be useful for any dynamic implementation, one should be able to actively control the cavity mode-splitting without any undesirable global shift of the split resonance. So far, the demonstrated controlling approaches are limited with respect to active tunability or resonance-shift. For example, counter-propagating mode-splitting induced by controlled sidewall gratings enables large and predictable mode-splitting [5], but it is not tunable. Tunable mode-splitting has been demonstrated using Mach–Zehnder interferometers to control the coupling strength between degenerate traveling wave resonators [10,11] with high-power efficiency, but at the price of resonance-shifts of the order of several FSRs. In practice, any tuning mechanism acting upon an optical path where the resonant optical field is highly confined will necessarily cause a significant change in the optical phase and lead to an undesirable resonance-shift.

In this Letter, we demonstrate the active control of mode-splitting in a multi-GHz range with very-low resonance shift in a coupled-cavity device. The large splitting and small resonance shift are simultaneously achieved through the controlled excitation of counter-traveling modes using embedded microrings. We compare our results with theoretical calculations and show that the performance of our fabricated device is only limited by thermal crosstalk.

We use a coupled microring device (Fig. 1) that allows for the controlled excitation of clockwise (CW) and counterclockwise (CCW) modes [8,12,13]. When the light launched into the bus waveguide ( $s_{in}$ ) is resonant with the embedded microrings ( $R_2$  and  $R_3$ ), both CW and CCW modes  $a_2^{CW,CCW}$  and  $a_3^{CW,CCW}$  are excited due to the direct coupling between these rings in the central region [Fig. 1(a)]. When the incident light is resonant with the outer microring ( $R_1$ ) only, it excites the CW mode  $a_1^{CW}$ . Neglecting CW-CCW coupling through sidewall roughness, the CCW mode  $a_1^{CCW}$  can be excited in the outer ring only if the detuning between embedded and outer microrings is small.  $R_2$  and  $R_3$  work as resonant back-reflectors, and the CW-CCW coupling induced mode-splitting can be dynamically controlled by acting on these microrings. Here we demonstrate this principle using the thermo-optic effect through integrated microheaters [Fig. 1(b)].

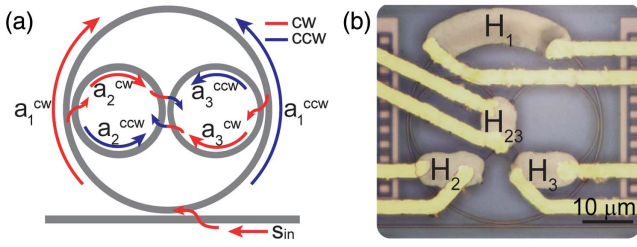


**Fig. 1.** Coupled microring device. (a) The direct coupling between two embedded microrings enables the excitation of CW- and CCW-traveling modes  $a_2^{CW,CCW}$  and  $a_3^{CW,CCW}$  even when the incident light  $s_{in}$  travels in one direction only. The coupling between  $a_1^{CW}$  and  $a_1^{CCW}$  is strong only if the detuning between outer and embedded rings is small. (b) Optical micrograph of the fabricated device with Ni-Cr microheaters.  $H_1$ ,  $H_2$ , and  $H_3$  tune each microring separately, while  $H_{23}$  allows to tune both embedded rings simultaneously.

We control the CW-CCW mode-splitting using two approaches that significantly reduce undesired resonance-shifts. This scheme is illustrated in Fig. 2 and relies on actuating either both embedded microrings simultaneously [Figs. 2(a) and 2(b)], or only one of them [Figs. 2(c) and 2(d)]. When  $R_2$  and  $R_3$  are initially blue-detuned with respect to  $R_1$  [Fig. 2(a)], heater  $H_{23}$  red-shifts the fourfold resonances of  $R_2$  and  $R_3$  toward the single-notch resonance of  $R_1$  (blue trace). A controllable CW-CCW mode-splitting is created as mode

$a_1^{CCW}$  is increasingly excited through the embedded rings, as shown in the blue-highlighted trace in Fig. 2(b). Alternatively, starting with the three coupled rings degenerate [Fig. 2(c)], all the six CW and CCW modes ( $a_{1,2,3}^{CW,CCW}$ ) are coupled, but only four resonance notches appear due to an accidental degeneracy [8]. Using heater  $H_3$  to red-shift only  $R_3$  effectively reduces the CW-CCW coupling for all supermodes [Fig. 2(d)]. Although the actuated ring supermodes strongly red-shift, the position of the remaining CW-CCW supermodes of cavities  $R_{1,2}$  (blue and green traces) are practically unaffected.

The proposed splitting control approaches feature-important advantages toward widely tunable splitting with no resonance shift. The controlled CW-CCW mode coupling is mediated by the coupling between microrings, therefore the maximum CW-CCW-induced splitting can be tailored through cavity design (gap separation and coupling length). On the other hand, the controlled mode-splitting can always be reduced to a single-notch resonance, since the uncoupled CW and CCW modes are degenerate. In both schemes described in Fig. 2, the resonance shifts are effectively mitigated as we minimize the overlap between the spatial distribution of the controlled supermodes (blue and green traces) and the cavity sections in which the refractive index is changed (around the orange heaters).

The passive optical device was fabricated on a SOI platform at IMEC-EUROPRACTICE with microring radius  $R_1 = 20 \mu\text{m}$ ,  $R_2 = R_3 = 9.625 \mu\text{m}$ , and a 200-nm coupling gap between each microring and between the outer microring and the bus waveguide. The waveguides dimensions are  $450 \text{ nm} \times 220 \text{ nm}$ , and the measurements were carried using their quasi-TE (transverse electric) mode. Microheaters and contact pads were fabricated in a post-process step using Ni-Cr and Ti/Au deposition (100 nm and 2/200 nm, respectively) and a photoresist lift-off process [14]. The measured electrical resistance of microheaters ( $H_1$ ,  $H_2$ ,  $H_3$ ,  $H_{23}$ ) were (275, 99, 107, 104)  $\Omega$ . Throughout the measurements, the voltage applied to the microheaters was kept below 2 V, compatible with CMOS voltage standards.

The experimental realization of the tuning approach using heater  $H_{23}$  demonstrates the generation and continuous tuning of mode splitting [Figs. 3(a) and 3(b)]. Starting from a single-notch resonance (loaded-Q of 6700), the splitting emerges at low heating power (7 mW) and increases almost linearly at a rate of roughly 1.8 GHz/mW [Fig. 3(d)] as the quadruplet resonances are red-shifted toward the outer ring resonance. From the uppermost trace in Fig. 3(b), we infer a resonance-splitting of approximately 30 GHz at 17.7 mW of heating power; further heating significantly changes the desired double-notch resonance splitting. A small resonance shift is observed in the transmission spectra (blue-dashed line) due to the mode anti-crossing dispersion and a small thermal crosstalk. This heating configuration shifts the embedded microring resonances at a rate of 9.5 GHz/mW, while a spurious shift of the outer ring resonance occurs at a rate of 1.5 GHz/mW due to the thermal crosstalk. To accurately measure the spurious shift, we used a spectral region (not shown in Fig. 3) where the embedded and outer rings resonances are uncoupled throughout the full range of heating power.

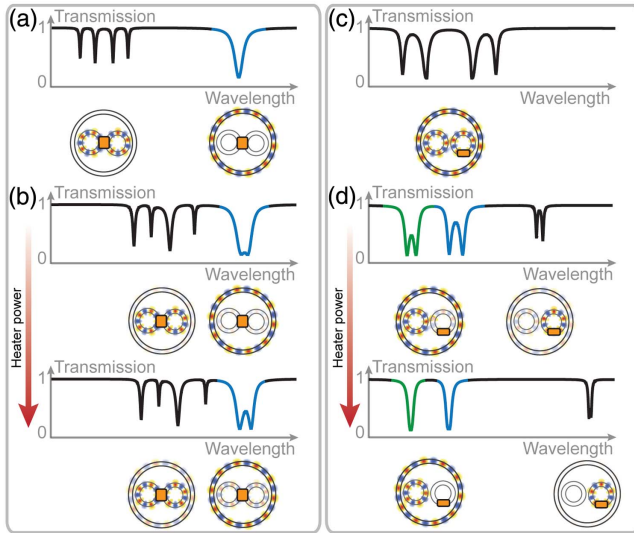


**Fig. 2.** Schematic of splitting control approaches using microheaters. The transmission traces show the resonances of the coupled cavity for different detuning conditions and the resonances in which mode-splitting is controlled (blue and green traces). The microring device below each resonance group depicts the spatial distribution of the associated supermodes and the actuated microheaters (orange rectangles). (a) Embedded and outer-ring supermodes are initially uncoupled. (b) The embedded ring resonances are simultaneously red-shifted toward the outer-ring resonance by means of heater  $H_{23}$ , increasing the CW-CCW mode-coupling in the outer ring. (c) Starting with the three microrings degenerate, (d) a single embedded ring is detuned using heater  $H_3$ , reducing the CW-CCW-induced mode-coupling for all supermodes.

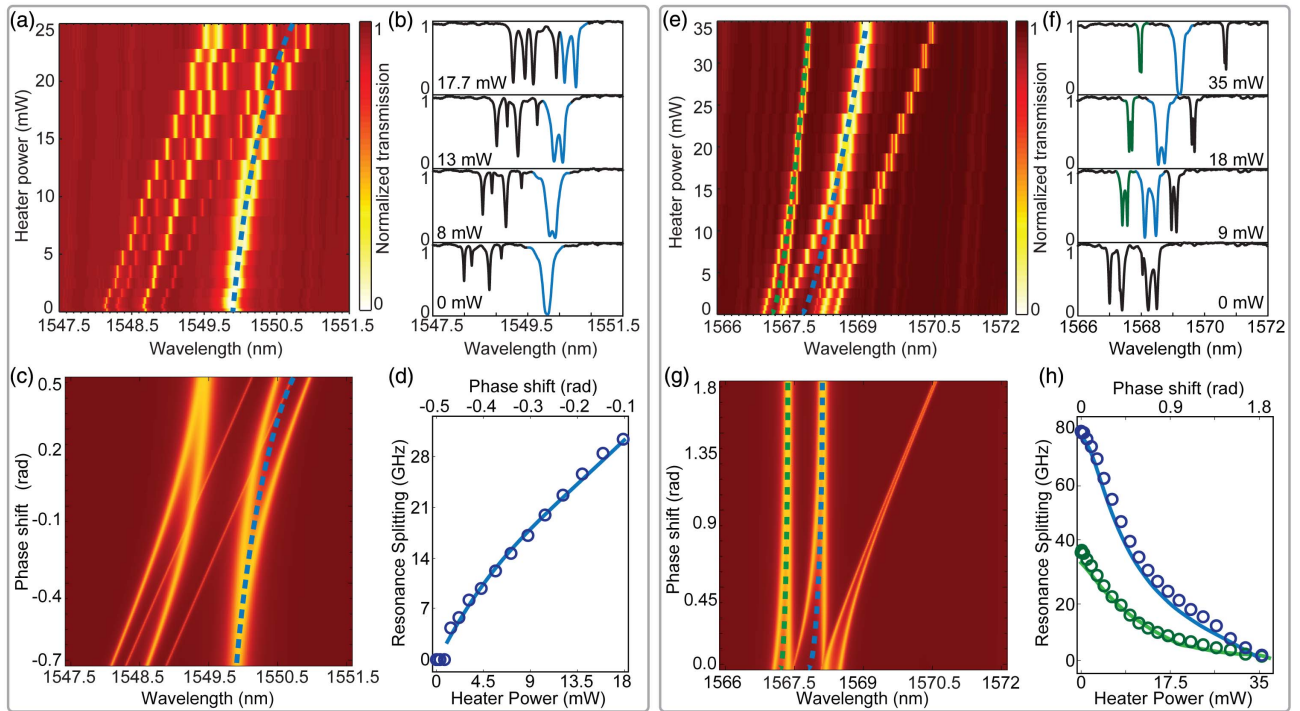


**Fig. 3.** Spectral evolution of the coupled-cavity resonances using heaters  $H_{23}$  (a)–(d) and  $H_3$  (e)–(h). (a) Measured and (c) calculated optical transmission as  $H_{23}$  power is increased. The blue-dashed line follows the central wavelength of the controlled resonance. (b) Transmission traces corresponding to specified heater powers. The blue color highlights the controlled resonance. (c) Calculated transmission as the phase of the embedded rings is simultaneously varied. (d) Experimental (circles) and calculated (line) resonance splitting as a function of the power dissipated in  $H_{23}$  and equivalent phase shift between embedded and outer rings (upper horizontal scale), respectively. (e) Measured and (g) calculated optical transmission as  $H_3$  power is increased. The blue- and green-dashed lines follow the central wavelength of the controlled resonances. (f) Transmission traces corresponding to specified heater powers. The blue and green color highlights the controlled resonances. (h) Measured (circles) and calculated (lines) resonance splitting for the set of split resonances, with green and blue indicating the leftmost and central resonances, respectively.

A qualitatively distinct tunable mode-splitting spectrum is observed when the three microrings are initially degenerate and only one embedded ring ( $R_3$ ) is actively detuned [Figs. 3(e) and 3(f)]. At low heating powers, the six supermodes exhibit a quasi-fourfold mode-splitting, highlighted in the bottom transmission trace in Fig. 3(f). As  $R_3$  is detuned, the coupling strength between CW and CCW modes gradually vanishes along with the associated mode splitting for all supermodes. The two resonances of interest are shown in Fig. 3(f) in green and blue traces. We show the resonance-splitting dependence on the heating power for these resonances in Fig. 3(h). Although this dependence is clearly nonlinear, this approach yields larger tunable splitting when compared to the previous one, with a maximum splitting of 80 GHz observed for the central (blue) resonance when the heater is off. On the other hand, this approach is also more severely affected by thermal crosstalk as indicated by the dashed lines in Fig. 3(e). Heater  $H_3$  shifts  $R_3$  at 8.7 GHz/mW, while thermal crosstalk impinges resonance-shifts of 1.56 GHz/mW in  $R_2$  and 4.6 GHz/mW in  $R_1$ .

We carried out calculations based on the transfer matrix method (TMM) to reproduce the supermode spectrum evolution and assess the impact of mode anti-crossing and thermal crosstalk on undesired resonance-shifts. By neglecting thermal

crosstalk in the TMM, we can identify the shifts caused only by mode anti-crossing dispersion. The TMM plot shown in Fig. 3(c) was obtained by simultaneously varying the two embedded rings' roundtrip phases ( $\phi_2$  and  $\phi_3$ , see Appendix A) and agrees very well with the experimental data of Fig. 3(a). Both the overall position of the controlled resonance (dashed lines) and the splitting evolution [Fig. 3(d), solid line] are well reproduced. This good agreement indicates that the small resonance shift observed in the experimental data is mostly affected by mode anti-crossing dispersion, i.e., the repulsion of the outer ring resonance by the approaching embedded ring resonances.

The TMM prediction indicates the great potential for resonance-shift-free, large-splitting control when only one embedded ring is detuned [Figs. 3(g) and 3(h)]. The almost dispersionless behavior of the controlled resonance set is emphasized by the dashed lines in Fig. 3(g). It shows that the mode anti-crossing dispersion remains much smaller than the splitting over the full control range. In addition, it confirms that the resonance shifts experimentally observed are indeed mostly due to thermal crosstalk.

We compare the performance of the two splitting control approaches in terms of the ratio resonance splitting over resonance shift. The experimental results yield splitting/shift ratios



of 0.46 using heater  $H_{23}$  and 0.42 and 0.54 for the blue and green resonances using heater  $H_3$  [Fig. 3(f)]. Ignoring the resonance shifts caused by thermal crosstalk, this values increase to 0.83, 2.67, and 2.53 for the three cases, respectively. Although clearly detrimental to this proof-of-principle demonstration, the effects of thermal crosstalk can be eliminated employing distinct dispersion control mechanisms such as carrier effects in silicon or electro-optic effects in other platforms, which exhibit extremely reduced crosstalk. Moreover, these mechanisms would enable low-power, ultrafast mode-splitting modulation.

In conclusion, we demonstrated reconfigurable mode-splitting control using a compact and power-efficient coupled-microring device. Experimental results show that resonances can be tuned from single notches to large mode splitting (80 GHz) with a minimum of resonance shift (limited by thermal crosstalk) through the controlled excitation of counter-propagating modes. We show that the proposed mechanism has the potential to deliver widely tunable mode splitting with extremely reduced resonance shifts. Further demonstrations using carrier effects instead of thermal tuning and diligent cavity designs may provide power-efficient ultrafast devices for applications such as reconfigurable optical filtering, single-sideband modulation and microwave photonics.

## APPENDIX A: TMM TRANSFER FUNCTION

The TMM curves were calculated using the following power transmission  $T$ , obtained using the matrix form of Mason's rule [15]:

$$T = \left| \frac{t_1 + \frac{A_1}{\chi_3} (t_1 A_1 \chi_1 + (1 + t_1^2) \chi_2)}{1 + t_1 \frac{A_1}{\chi_3} (t_1 A_1 \chi_1 + 2\chi_2)} \right|^2, \quad (\text{A1})$$

where  $A_i = a_i e^{j\phi_i}$  is the field propagation factor of microring  $i$  ( $i = 1, 2, 3$ ), with  $a_i$  and  $\phi_i = (2\pi/\lambda)L_i n_{\text{eff}}(\lambda)$  representing the round-trip attenuation factor and accumulated phase shift.  $L_i$  is the perimeter of microring  $i$ , and a first-order approximation of the effective index is assumed,  $n_{\text{eff}}(\lambda) \approx n_{\text{eff}}(\lambda_0) + (\lambda - \lambda_0) \partial n_{\text{eff}}(\lambda_0) / \partial \lambda$ . The  $\chi_i$  coefficients are given by

$$\chi_1 = ((A_2 - t_2 t_{23})(A_3 - t_3 t_{23}) + t_2 t_3 \kappa_{23}^2)^2$$

$$\begin{aligned} \chi_2 = & \sqrt{t_2 t_3} t_{23} (1 + t_2 t_3) (A_2 + A_3) (A_2 A_3 + 1) \\ & + A_2 A_3 (t_2^2 t_3^2 + 1) \\ & \times (1 - 2t_{23}^2) - t_2 t_3 (t_{23}^2 (A_2 - A_3)^2 + A_2 A_3 (A_2 A_3 + 4) + 1) \end{aligned}$$

$$\chi_3 = ((A_2 t_2 - t_{23})(A_3 t_3 - t_{23}) + \kappa_{23}^2)^2,$$

where the field transmission and coupling coefficients ( $t_i, \kappa_i$ ) respect the lossless coupling condition  $t_i^2 + \kappa_i^2 = 1$  and represent the coupling between outer ring and bus waveguide ( $t_1, \kappa_1$ ), embedded rings and outer ring ( $t_2, \kappa_2, t_3, \kappa_3$ ), and between embedded rings ( $t_{23}, \kappa_{23}$ ). The attenuation factors

( $a_1, a_2, a_3$ ) and coupling coefficients ( $\kappa_1, \kappa_2, \kappa_3, \kappa_{23}$ ) used in Figs. 3(c) and 3(g) were (0.965, 0.994, 0.994) and (0.47, 0.345, 0.345, 0.2), respectively. The parameters ( $n_{\text{eff}}(\lambda_0)$ ,  $\partial n_{\text{eff}}(\lambda_0) / \partial \lambda$ ,  $\lambda_0$ ) used to calculate the accumulated phase in Figs. 3(c) and 3(g) were (2.306,  $-1.22 \times 10^{-3} \text{ nm}^{-1}$ , 1549.5 nm) and (2.295,  $-1.22 \times 10^{-3} \text{ nm}^{-1}$ , 1568 nm), respectively. An additional term  $\delta\phi$  was introduced to  $\phi_2$  and  $\phi_3$  in Fig. 3(c) and to  $\phi_3$  in Fig. 3(g), accounting for the phase shift in the theoretical plots. These parameters were obtained adjusting the calculated transmission traces to the experimental data around the spectral region of interest.

**Funding.** Conselho Nacional de Desenvolvimento Científico e Tecnológico (National Council for Scientific and Technological Development) (08/57857-2); Fundação de Amparo à Pesquisa do Estado de São Paulo (São Paulo Research Foundation) (2012/17765-7, 2014/04748-2).

**Acknowledgment.** The authors acknowledge T. P. M. Alegre for fruitful discussion and the Brazilian Nanotechnology National Laboratory (LNNano) during the fabrication process.

## REFERENCES

1. A. Willner, S. Khaleghi, M. Chitgarha, and O. Yilmaz, *J. Lightwave Technol.* **32**, 660 (2014).
2. T. Claes, J. Molera, K. De Vos, E. Schachtb, R. Baets, and P. Bienstman, *IEEE Photon. J.* **1**, 197 (2009).
3. T. J. Kippenberg, R. Holzwarth, and S. A. Diddams, *Science* **332**, 555 (2011).
4. C. M. Gentry, X. Zeng, and M. A. Popovi, *Opt. Lett.* **39**, 5689 (2014).
5. X. Lu, S. Rogers, W. C. Jiang, and Q. Lin, *Appl. Phys. Lett.* **105**, 151104 (2014).
6. L. A. M. Barea, F. Vallini, P. F. Jarschel, and N. C. Frateschi, *Appl. Phys. Lett.* **103**, 201102 (2013).
7. Q. Chang, Q. Li, Z. Zhang, M. Qiu, T. Ye, and Y. Su, *IEEE Photon. Technol. Lett.* **21**, 60 (2009).
8. M. C. M. Souza, L. A. M. Barea, F. Vallini, G. F. M. Rezende, G. S. Wiederhecker, and N. C. Frateschi, *Opt. Express* **22**, 10430 (2014).
9. Q. Li, Z. Zhang, J. Wang, M. Qiu, and Y. Su, *Opt. Express* **17**, 933 (2009).
10. A. H. Atabaki, B. Momeni, A. A. Eftekhari, E. S. Hosseini, S. Yegnanarayanan, and A. Adibi, *Opt. Express* **18**, 9447 (2010).
11. X. Sun, L. Zhou, J. Xie, Z. Zou, L. Lu, H. Zhu, X. Li, and J. Chen, *IEEE Photon. Technol. Lett.* **25**, 936 (2013).
12. M. Souza, L. Barea, G. Wiederhecker, A. von Zuben, and N. Frateschi, in *Conference on Laser and Electro-Optics*, OSA Technical Digest (online) (Optical Society of America, 2015), paper JTU5A.49.
13. J. Poon, J. Scheuer, and A. Yariv, *IEEE Photon. Technol. Lett.* **16**, 1331 (2004).
14. W. S. Fegadolli, G. Vargas, X. Wang, F. Vallini, L. A. M. Barea, J. E. B. Oliveira, N. Frateschi, A. Scherer, V. R. Almeida, and R. R. Panepucci, *Opt. Express* **20**, 14722 (2012).
15. S. J. Mason, *Proc. IRE* **44**, 920 (1956).